Earth and Space Science

RESEARCH ARTICLE
10.1029/2023EA003071

Key Points:

- The 14-panel Advanced Modular Incoherent Scatter Radar 2D representation is well-suited for studies of the plume generation, dynamics, and decay
- Even during mild storms/substorms the recurrent penetration of electric fields seems to impact the equatorial ionosphere phenomenology
- The mechanism proposed by Abdu et al. (1998) properly explains the reversal in the zonal drift of the Equatorial Plasma Bubbles/plumes over distinct longitudes. The contribution from the Hall conductivity seems to dominate over the contribution from the vertical current

Supporting Information:

Supporting Information may be found in the online version of this article.

Correspondence to:

J. Sousasantos,
jonas.ssts@utdallas.edu

Citation:

Sousasantos, J., Rodrigues, F. S., Fejer, B. G., Abdu, M. A., Massoud, A. A., & Valladares, C. E. (2023). On the role of mild substorms and enhanced hall conductivity in the plasma irregularities onset and zonal drift reversals: Experimental evidence at distinct longitudes over South America. *Earth and Space Science*, *10*, e2023EA003071. https://doi.org/10.1029/2023EA003071

Received 27 MAY 2023
Accepted 14 OCT 2023

On the Role of Mild Substorms and Enhanced Hall Conductivity in the Plasma Irregularities Onset and Zonal Drift Reversals: Experimental Evidence at Distinct Longitudes Over South America

J. Sousasantos[1], F. S. Rodrigues[1], B. G. Fejer[2], M. A. Abdu[3], A. A. Massoud[1], and C. E. Valladares[1]

[1]William B. Hanson Center for Space Sciences, University of Texas at Dallas (UTD), Richardson, TX, USA, [2]Center for Atmospheric and Space Sciences, Utah State University, Logan, UT, USA, [3]Instituto Nacional de Pesquisas Espaciais, São José dos Campos, Brazil

Abstract The 14-panel Advanced Modular Incoherent Scatter Radar (AMISR-14) system deployed at Jicamarca observed equatorial spread F plumes on two consecutive nights under unfavorable seasonal and solar flux conditions during a period that can be categorized as geomagnetically quiet. The AMISR-14 capability of observing in multiple pointing directions allowed the characterization of the irregularity zonal drifts revealing that, in addition to their atypical occurrence, the zonal drifts of these plumes/irregularities also presented distinct patterns from one night to another, reversing from east to west on the second night. This work addresses two main subjects: (a) the mechanisms that may have led to the generation of these irregularities, despite the unfavorable conditions, and (b) the mechanisms that possibly led to the reversal (east-to-west) in the zonal plasma drift on the second night. To do so a multi-instrumented and multi-location investigation was performed. The results indicate the occurrence of simultaneous spread-F events over the Peruvian and the Brazilian regions, evidencing a non-local process favoring the development of the irregularities. The results also suggest that, even under very mild geomagnetic perturbation conditions, the recurring penetration of electric fields in the equatorial ionosphere can occur promptly, modifying the equatorial electrodynamics and providing favorable conditions for the plume development. Moreover, the results confirm that the eastward penetration electric fields, combined with the upsurge of Hall conductivity in the nighttime typically associated with the presence of sporadic-E layers, are likely to be the mechanism leading to the reversal in the irregularity zonal drifts over these regions.

1. Introduction

The occurrence of plasma irregularities over low latitudes during nighttime is very often captured by instruments probing the ionosphere. These irregularities are characterized by severe density depletions, leading to steep gradients. Climatological studies revealed that these irregularities, also referred to as spread-F (ESF), plumes, or Equatorial Plasma Bubbles (EPBs), are more likely to develop over the Peruvian sector during September–April (Chapagain et al., 2009) and over the Brazilian region in the months of October-March (Sobral et al., 2002). However, sometimes these structures develop during June–August months over varied longitudes including South America (Li et al., 2011; Rodrigues et al., 2018) and more often India (Chandra & Rastogi, 1972; Patra et al., 2009; Sastri, 1999; Subbarao & Krishnamurthy, 1994), Africa (Yizengaw et al., 2013) and Indonesia (Ajith et al., 2015, 2016). The atypical events over South America during June solstice usually occur during "geomagnetic disturbed periods" and are attributed to changes in the equatorial electrodynamics due to the contribution of strong geomagnetic storms and substorms through mechanisms such as the disturbance dynamo (Blanc & Richmond, 1980; Fejer et al., 2017) and the prompt penetration electric fields (Fejer & Navarro, 2022; Fejer et al., 2021; Senior & Blanc, 1984; Spiro et al., 1988). Some works have shown the occurrence of EPBs during June solstice months under geomagnetic quiet conditions (e.g., Paulino et al., 2010; Sobral et al., 2011; Zhan & Rodrigues, 2018).

Under geomagnetic quiet conditions, the zonal motion of ionospheric irregularity structures (e.g., EPBs) is known to be predominantly eastward throughout the night, which agrees with the zonal motion of the background ionospheric plasma (Fejer et al., 1985, 2013; Valladares et al., 1996; Vargas et al., 2020). However,

Author Contributions:

Conceptualization: J. Sousasantos, F. S. Rodrigues, B. G. Fejer, M. A. Abdu
Data curation: C. E. Valladares
Formal analysis: J. Sousasantos, F. S. Rodrigues, A. A. Massoud
Funding acquisition: F. S. Rodrigues
Investigation: J. Sousasantos, M. A. Abdu
Methodology: J. Sousasantos, M. A. Abdu
Project Administration: F. S. Rodrigues
Software: J. Sousasantos, A. A. Massoud
Supervision: J. Sousasantos, F. S. Rodrigues
Validation: J. Sousasantos
Visualization: J. Sousasantos
Writing – original draft: J. Sousasantos
Writing – review & editing: J. Sousasantos, F. S. Rodrigues, B. G. Fejer, M. A. Abdu, A. A. Massoud, C. E. Valladares

during geomagnetic disturbed periods the direction of the EPB motion sometimes reverses to the west (Abdu et al., 1998, 2003; Fejer & Scherliess, 1998; Paulino et al., 2010).

There are several processes that may lead the zonal drift to become westward, including the reversal in the quiet-time thermospheric winds (Sobral et al., 2011), the thermospheric disturbance winds and the storm-time disturbance dynamo electric fields (Blanc & Richmond, 1980; Navarro & Fejer, 2019, 2020), and the combination of prompt-penetration electric fields and a persisting Hall conductivity (Abdu et al., 1998, 2003).

In this work, data from two nights during the solar minimum (85.7 sfu $\leq F10.7 \leq$ 92.4 sfu) June solstice (August 30–31, 2021, and August 31–1 September 2021) were analyzed using measurements made by the AMISR-14 radar deployed at Jicamarca. To aid the analysis, data from ionosondes/Digisondes over Peru/Brazil and all-sky imagers over Brazil were also employed. On both nights the instruments observed the occurrence of atypical plumes/EPBs with distinct zonal drift characteristics. At first glance the nights could be classified as geomagnetically quiet, but a more careful inspection indicates evident resemblances between parameters of the geospace and of the equatorial ionosphere, suggesting that even under considerably mild geomagnetic disturbances the low-latitude electrodynamics may be altered by recurring penetration of electric fields, possibly due to substorms. Motivated by these initial findings, a multi-instrumental and multi-location approach was employed in this work to achieve a better understanding about the mechanisms that possibly favored the development of plumes/EPBs under adverse seasonal conditions and the processes that may have led to the reversal in the zonal drift on the second night. The next section presents details regarding the stations and instruments used. After that, the results are discussed in detail.

2. Stations and Instruments

In this work, data from instruments deployed over the Peruvian sector (western coast of South America) were accompanied by ancillary data from instruments over the Brazilian region (eastern coast of South America) to evaluate the electrodynamic changes operating over distinct longitudes during atypical ESF/EPB events between August 30–1 September 2021.

The main data set used in this work are Range-Time-Intensity (RTI) maps obtained from the AMISR-14 system operating in the ESF mode at the Jicamarca Radio Observatory. Detailed information about the system can be found in Rodrigues et al. (2015). Rodrigues et al. (2015) demonstrated the ability of the system to provide a two-dimensional view of ESF phenomena. In their work, a total of five beams were pointed perpendicular to the geomagnetic equator on the magnetic equatorial plane (east-west). After repairs to the system that occurred during 2019–2021 the AMISR-14 was set to execute new two-dimensional observations of ESF events. These new observations were performed using 10 pointing directions in the magnetic equatorial plane, as depicted in Figure 1, covering approximately 400 km in the east-west direction at the altitudes of the F region. More details about the location of the system and the azimuth and elevation angles of the beams are presented in Table 1. The RTI maps using this unique feature of distinct pointing directions allowed the identification of zenith and off-zenith plume structures, indicating the occurrence of ESF/EPBs while also supporting the analysis of their dynamics.

To evaluate the ionospheric background characteristics over Jicamarca during the two events analyzed in this work, ionograms from the Vertical Incidence Pulsed Ionospheric Radar (VIPIR) deployed at the Jicamarca Radio Observatory were also used.

As mentioned earlier, the analysis presented in this work also employed data available from instruments deployed at low-latitude stations distributed over the Brazilian region. This was done to enable a comparison between the ionospheric electrodynamic changes over the westernmost (Peru) and easternmost (Brazil) portions of South America. These two regions are also in the "opposite boundaries" of the South Atlantic Magnetic Anomaly (SAMA), making them suitable to observe whether certain physical processes change over each location. By carrying out this comparison, this work aims to provide a better understanding about the mechanisms operating over the nighttime low-latitude ionosphere during mild geomagnetic substorms. Images captured by all-sky imagers deployed in Cachoeira Paulista and São Martinho da Serra were used to inspect the occurrence and the dynamics of the EPBs over the eastern coast of South America. To assess the ionospheric background characteristics during the events, data from Digisondes deployed over Fortaleza, São Luís, and Cachoeira Paulista were

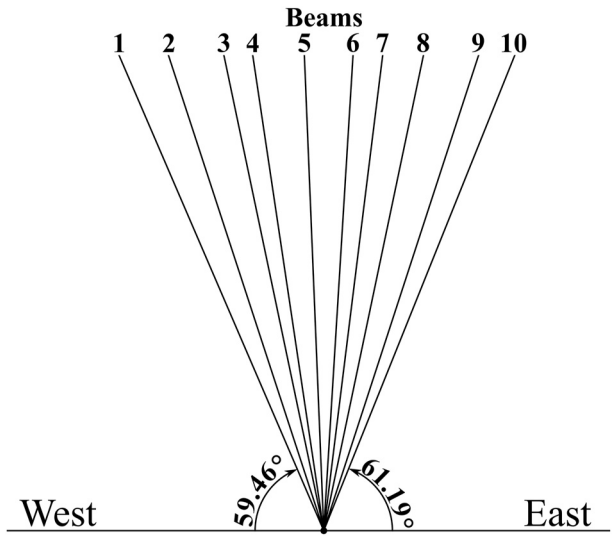

Figure 1. Pictorial description of the 14-panel Advanced Modular Incoherent Scatter Radar antenna beam positions over the magnetic equatorial plane during the observations reported in this work.

also used so that ionospheric background characteristics over Peru and Brazil could be compared. The coordinates of all the stations and instruments used in this work are provided in Table 1.

To facilitate the visualization of the spatial distribution of the instruments used in this work Figure 2 was prepared. Please note that all the instruments are embedded in the region under influence of the SAMA.

The geomagnetic field intensity and dip latitude were obtained using the IGRF-13 (Alken et al., 2021). The solar flux and geomagnetic indices were obtained from the National Aeronautics and Space Administration (NASA) Space Physics Data Facility (SPDF) OMNIWeb (King & Papitashvili, 2005).

3. Results and Discussion

As previously mentioned, the occurrence of ESF/EPBs over the Southern American sector during June solstice months is atypical. These June solstice ESF/EPBs are, most of the time, observed during low-solar flux conditions and under geomagnetic storm/substorm influences. They typically grow at later hours in the night when compared to events that arise in equinoctial and December solstice months (Rodrigues et al., 2018). The decreased occurrences and, sometimes, the complete absence of these irregularities during these months are attributed to the negligible magnitude of the vertical drift, that is, virtual lack of the pre-reversal enhancement of the zonal (eastward) electric field in the dusk sector (Smith et al., 2016). Since the growth rate of the generalized Rayleigh-Taylor instability that generates the plasma irregularities depends on the vertical component of the plasma drift (ExB), it is drastically reduced (Kelley, 1989; Ossakow et al., 1979; Sultan, 1996). In addition to that, the weak upward drifts cause the ionospheric F-region to stay at lower altitudes, where chemical loss is more efficient. Moreover, the collision frequency (ν_{in}) at lower altitudes is larger, decreasing the gravity driven term (g/ν_{in}) in the growth rate as well. Therefore, even if a seeding

Table 1
Location of the Stations and Instruments Used in This Work

Station	Instrument(s)	Geographic longitude	Geographic latitude	Dip latitude
Jicamarca	AMISR-14	76.87°W	11.95°S	0.61°S
	Beam #: Azimuth; Elevation			
	Beam 1: −95.20°; 59.50°			
	Beam 2: −96.50°; 65.80°			
	Beam 3: −97.70°; 73.80°			
	Beam 4: −99.50°; 78.30°			
	Beam 5: −108.40°; 86.60°			
	Beam 6: 102.5°; 85.10°			
	Beam 7: 93.20°; 80.40°			
	Beam 8: 90.00°; 74.00°			
	Beam 9: 90.00°; 66.20°			
	Beam 10: 88.90°; 61.20°			
	VIPIR (ionosonde)			
São Luís	Digisonde	44.30°W	2.54°S	4.78°S
Fortaleza		38.54°W	3.72°S	9.07°S
Cachoeira	All-sky imager	45.01°W	22.67°S	21.51°S
Paulista	Digisonde			
São Martinho da Serra	All-sky imager	53.83°W	29.45°S	21.66°S

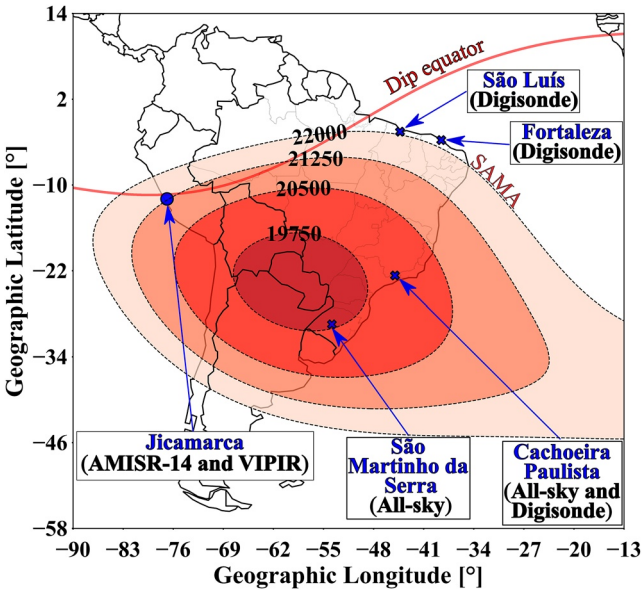

Figure 2. Location of the stations and instruments used (blue markers) and the South Atlantic Magnetic Anomaly (SAMA) isocontours (red) during 2021. The values of the geomagnetic field intensity are in nT. All the instruments were deployed in regions under the influence of the SAMA.

source disturbance is available (e.g., gravity waves, large-scale wave structures, etc.), the attenuated growth rate is unlikely to produce topside structures under these unfavorable conditions.

In the following sections, data from two nights, August 30–31, 2021, and August 31–1 September 2021, are analyzed. These nights were chosen because AMISR-14 observed the occurrence of RTI plumes (i.e., EPBs) over Jicamarca on both nights. More importantly, the 2D capabilities of the AMISR-14 system revealed that these EPBs/irregularities behaved in considerably distinct ways. There are two main subjects that will be addressed in this work: (a) the mechanisms that may have led to the generation of these EPB events, despite the typical unfavorable conditions, and (b) the underlying mechanisms that possibly led to the reversal (east-to-west) in the zonal plasma drift on the second night (August 31–1 September 2021).

4. On the Conditions Leading to the Atypical Occurrence of Equatorial Plasma Bubbles

The first analysis aims to identify possible mechanisms favoring to the occurrence of ESF/EPBs under adverse seasonal and solar flux conditions. Figure 3 shows the RTI maps from AMISR-14 for August 30–31, 2021, with beams 1–10 (upper to lower panels) representing data from west to east, respectively. For Jicamarca, LT ≈ UT-5.12, therefore, the panels from 18:00 LT up to 02:00 LT correspond to approximately 23:08 UT up to 07:08 UT. The panel showing the data closest to the zenith (beam 5) also displays gray lines describing an approximate vertical drift (Vz) estimated from the VIPIR ionograms (Vz = dhF/dt) with values indicated on the vertical axis at the right-hand side. On this night, the frequencies of 4–6 MHz were used. The median of the vertical drifts estimated with the frequencies 4–6 MHz at the same night was also calculated and is shown in red. The vertical drift as estimated by the model of Scherliess and Fejer (1999) - SF1999 is also included (magenta line). The SF1999 model produces accurate climatological estimates of the vertical plasma drift over Jicamarca (e.g., see Figure 2 of Shidler et al., 2019), and the model result was included to highlight how much the estimated Vz deviated from the expected climatological values on that night.

The beams pointed more to the west (upper panels) reveal the presence of a steady bottom-type structure more evident after 20:30 LT. Later, at 21:30 LT, a more developed scattering structure is observed evolving into a topside plume while drifting to the east. The black dashed line demarcates the approximate time when the plume was first perceived by each beam, revealing the dynamic behavior of the evolution and its eastward drift (i.e., the structure was observed slightly later as more eastward beams are considered). Previous studies have shown that under similar solar flux conditions (85.7 sfu ≤ F10.7 ≤ 92.4 sfu) these unusual plumes during June solstice tend to occur late in the evening (Chapagain et al., 2009).

According to the vertical drift predicted by the SF1999 for the hours presented in the panels of Figure 3, Vz should be very small, decreasing smoothly from ∼5 m/s (around 18:00 LT) down to ∼−18 m/s (around 21:45 LT). Vz estimated using the VIPIR data, however, reveals a considerably different behavior, being predominantly positive after 18:30 LT and exhibiting two steep increases. First, Vz increased from ∼−12 m/s up to ∼17 m/s between ∼18:00 LT–18:30 LT. After that it decayed, with intermittent oscillations between ∼18:30 LT and 20:30 LT. In the sequence, a second increase takes place, and Vz rises from ∼ −2 m/s (about 20:30 LT) up to ∼22 m/s (around 21:22 LT). The time in which the second rise initiates coincides with the bottom-type structure captured by the AMISR-14 system, and the subsequent plume development took place approximately 30 min after the peak of the second increase in Vz.

The magnitude of the upgrowth in Vz and the fact that the plume rises approximately when Vz is reversing (i.e., the time of the F-region peak height) conform with the conditions needed for an initial instability to evolve into a plume (Abdu et al., 1983, 2009; Huang, 2018; Jayachandran et al., 1993). More specifically, Vz is predominantly positive after ∼18:00 LT, hence, the F-region is consistently uplifted over the early nighttime hours, providing significant ExB contribution while also increasing the gravity-driven term in the growth rate. Therefore, once the

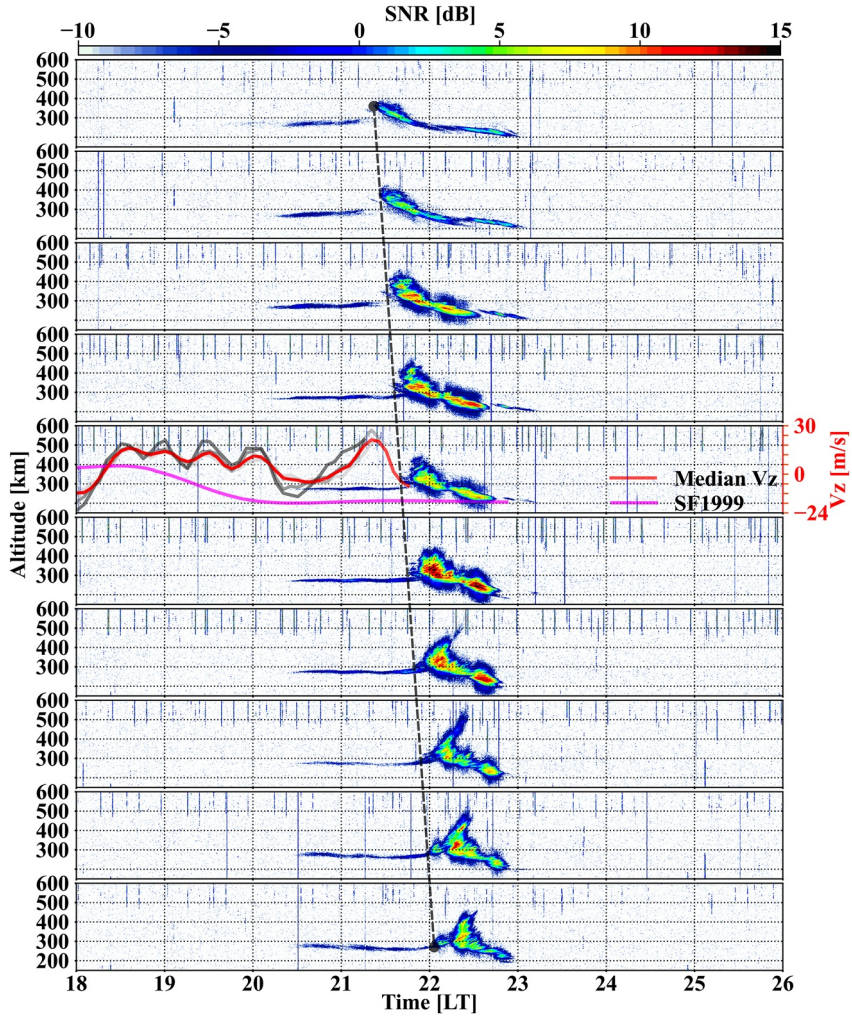

Figure 3. Range-Time-Intensity maps from 14-panel Advanced Modular Incoherent Scatter Radar beams 1–10 (upper to lower panels) for 30–31 August 2021. The beams from 1 to 10 correspond to data from west to east, respectively. The black dashed line across the panels highlights the eastward motion of the plumes with time. The gray lines in the panel of beam five indicate the vertical drift estimated from the Vertical Incidence Pulsed Ionospheric Radar data considering the available frequencies at that period (4–6 MHz), and the red line corresponds to its median value. The magenta line represents the SF1999 model.

instability is seeded in the bottomside, it will find favorable conditions to erupt upward. The noteworthy aspect, nonetheless, is that these conditions are atypical for June solstice period.

A geomagnetic storm occurred a few days earlier, but between August 30–31, 2021, the planetary index Kp maximum value was 2.7, and the Disturbance storm time index (Dst) minimum value was −24 nT. Typically, a weak storm requires Kp ≥ 4 and Dst ≤ −36 nT (Loewe & Prölss, 1997). Based on these indices, one would classify the period as geomagnetically quiet, however, additional data suggests that some mild substorms may have happened. The initial estimates of the Auroral Electrojet (AE) index ("quicklook" version available at https://wdc.kugi.kyoto-u.ac.jp/ae_realtime/index.html) were small but indicate increases of about ∼500 nT at ∼22:50 UT (∼17:45 LT at Jicamarca) and ∼02:30 UT (∼21:23 LT at Jicamarca) on August 30–31, 2021. The provisional data for the period of interest is not yet available for download. Further analysis also reveals interesting resemblances between other geospace parameters and the observed behavior in the equatorial ionosphere as illustrated in Figure 4.

The upper, middle, and lower panels of Figure 4 show the interplanetary magnetic field (B_z), the interplanetary electric field component (E_y), and the vertical drift over Jicamarca, respectively. B_z turned southward (i.e., $B_z < 0$) around 22:50 UT (17:45 LT), and, after that, it reached maximum southward values (indicated by the blue

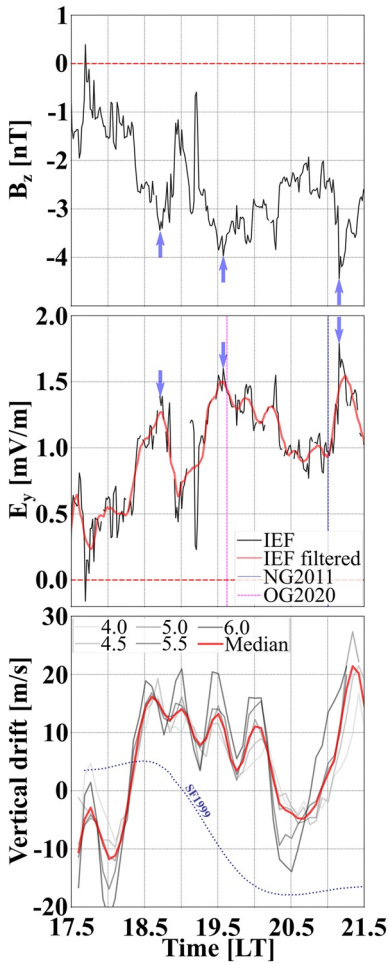

Figure 4. Interplanetary magnetic field—B_z (upper panel), interplanetary electric field—E_y (middle panel), and the vertical drift estimated from Vertical Incidence Pulsed Ionospheric Radar data (lower panel) on 30–31 August 2021. The blue arrows in B_z/E_y highlight instants of maximum southward/eastward values. The magenta and blue dashed lines indicate the instant of substorms onsets according to the NG2011 and OG2020 approaches, respectively.

arrows). Each one of these maximum southward occurrences in B_z coincides with maximum eastward E_y (middle panel), also highlighted by blue arrows. The first and the last B_z southward drops occurred approximately at the same time as the increases in AE mentioned earlier. The two last southward peaks could also be related to substorm onsets according to the Newell and Gjerloev (2011) and Ohtani and Gjerloev (2020) approaches, respectively. It must be mentioned, however, that the electrodynamics is complex and may involve additional mechanisms. The substorm onsets according to the Newell and Gjerloev (2011)—NG2011 and Ohtani and Gjerloev (2020)—OG2020 are represented, respectively, by the magenta and blue dashed lines in the middle panel.

One distinguishable aspect in Figure 4 is the resemblance between the increases in the eastward E_y and in the vertical drift over the equatorial region during the predominantly southward B_z condition. A smoothed version of E_y (red solid line) was introduced in the middle panel to facilitate the visualization of its behavior. First E_y increased from ∼0 up to ∼1.4 mV/m between 17:45 LT and 18:45 LT. After that, it decreased during 19:30 LT–20:45 LT. In the sequence it rises again from ∼0.75 mV/m up to ∼1.8 mV/m between 20:45 LT–21:15 LT. If the lower panel is now considered, one may readily notice that the pattern in the vertical drift was considerably similar, increasing steeply during both rises of eastward E_y and decreasing with the decrease in E_y as well. Even an oscillatory pattern seems to be present in both quantities during the decrease of their respective magnitudes. These results can possibly indicate that, even under mild geomagnetic perturbations, recurring penetration of electric fields from storms and substorms in the equatorial ionosphere can modify promptly and significantly the transport and the related plasma phenomena, possibly favoring the ESF/EPB development.

Figure 5 shows another example, with RTI maps from the next night (August 31–1 September 2021) from the 10 beams of the AMISR-14 system and the vertical drift estimated from the VIPIR ionograms. The graphical elements are the same as in Figure 3, but this time one can notice that there are two black dashed lines. The second black dashed line indicates a reversal in the zonal drift. The first plume, that was first observed around 21:45 LT by the westernmost beam (beam 1), drifts to the east. However, the irregularity structure (bottom-side ESF) that appeared around 23:30 LT in the easternmost beam (beam 10) drifts westward.

The estimated vertical drift, as in the previous case, was predominantly positive, except during a period between ∼20:45 LT and 21:45 LT. In any case, it was, most of the time, considerably larger than what was expected (i.e., SF1999 model). Analogously to the previous case, the larger vertical drift (mostly upward) may have provided favorable conditions for bottomside irregularities to grow vertically.

Regarding the geomagnetic conditions, the maximum value for Kp and the minimum value for Dst during August 31–1 September 2021, were equal to the ones previously mentioned. The AE index (i.e., the "quicklook" version) during the night was small, suggesting the absence of substorms. However, according to the criteria of NG2011 and OG2020, some substorms happened during that night.

Figure 6 presents three panels with the same graphical elements previously employed in Figure 4. The upper panel shows that after ∼19:00 LT (∼00:07 UT on September 1) B_z turned southward and remained predominantly to the south with four maximum southward peaks (blue arrows). Each maximum southward incursion in B_z is, again, accompanied by an increase in the eastward component E_y (middle panel), as indicated by the blue arrows.

The noteworthy aspect is that, although one would classify this night as a quiet night according to the geomagnetic indices Kp, Dst, and AE, the general trend in the E_y seems to be promptly manifested also in the equatorial vertical drift. This would suggest that penetration of electric fields from magnetospheric events may occur more

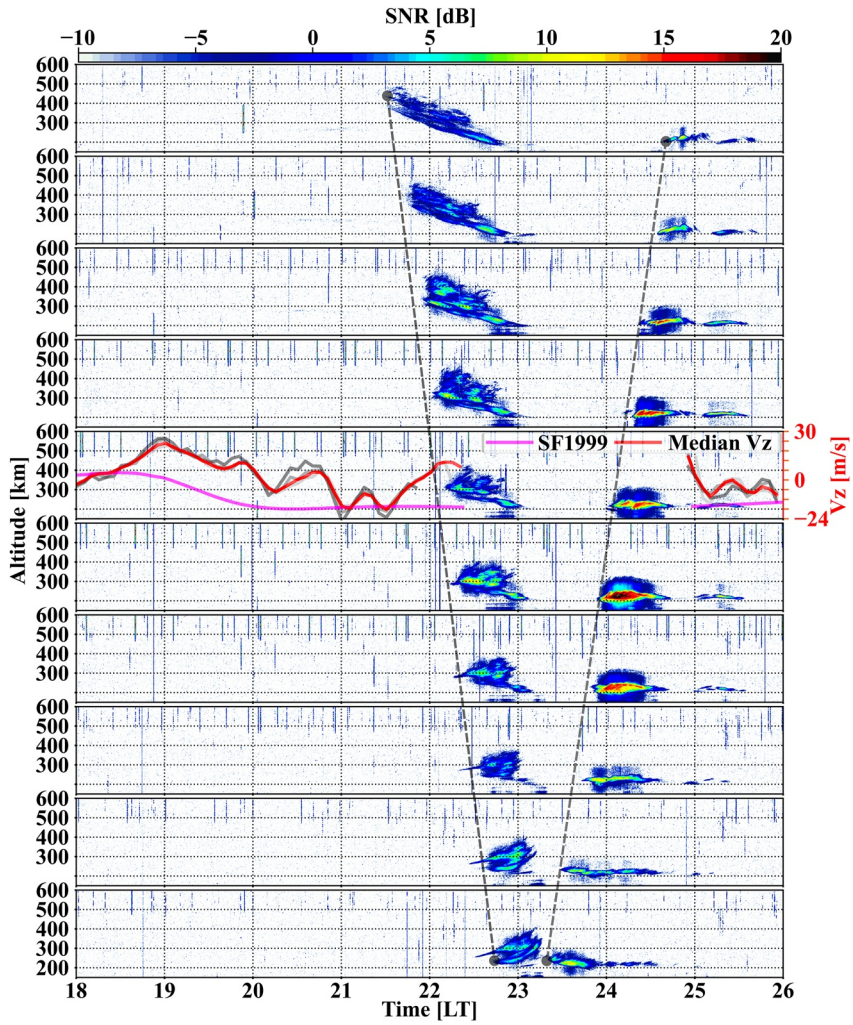

Figure 5. Range-Time-Intensity maps from 14-panel Advanced Modular Incoherent Scatter Radar beams 1–10 (upper to lower panels) for August 31–1 September 2021. The beams from 1 to 10 correspond to data from west to east, respectively. The black dashed lines across the panels highlight the eastward/westward motion of the first/second plume/irregularity with time. The gray lines in the panel of beam five indicate the vertical drift estimated from the Vertical Incidence Pulsed Ionospheric Radar data considering the available frequencies at that period (3–4.5 MHz), and the red line corresponds to its median value. The magenta line represents the SF1999 model.

often than previously thought. Additionally, it would indicate that recurring substorms associated with storm-time can contribute to changing considerably the electrodynamics over low latitudes. Obviously, there are other complex processes occurring at the same time, but the resemblance of the trends of E_y and Vz are noteworthy. It is reasonable to suggest that effects of these mild substorms may possibly have provided the conditions that led to the atypical occurrence of ESF/EPB during these nights of winter solstice. It must be also mentioned that the NG2011 and OG2020 approaches were able to identify substorm onsets that otherwise would have been neglected.

5. On the Experimental Evidence of Non-Local Mechanisms Favoring the ESF/EPB Development

In the previous section, the possible mechanisms leading to the unexpected occurrence of the plumes observed by the AMISR-14 system were discussed. It is interesting to notice, however, that the events had dissimilarities, despite the mechanisms contributing to their generation being, possibly, the same. The most noticeable difference is the zonal component of the irregularity drift that was discernible due to the 2D observational capabilities of the AMISR-14.

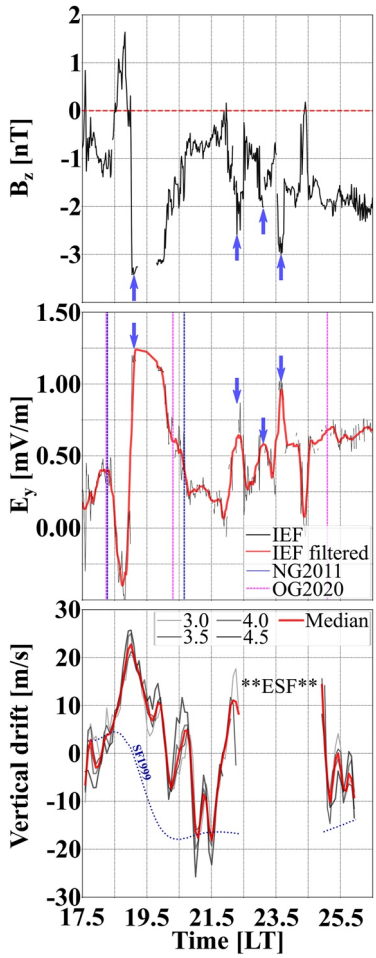

Figure 6. Interplanetary magnetic field—B_z (upper panel), interplanetary electric field—E_y (middle panel), and the vertical drift estimated from Vertical Incidence Pulsed Ionospheric Radar data (lower panel) in August 31–1 September 2021. The blue arrows in B_z/E_y highlight instants of maximum southward/eastward values. The magenta and blue dashed lines indicate the instant of substorms onsets according to the NG2011 and OG2020 approaches, respectively.

On the night of 30–31 August 2021, the irregularity zonal drift over Jicamarca was eastward (see Figure 3). Around the same time in which this plume was drifting eastward, an EPB structure was observed over Brazil and was also drifting eastward. The images from the all-sky imager deployed in Cachoeira Paulista were cloudy, but the all-sky imager deployed in São Martinho da Serra (see Table 1 and Figure 1) recorded this EPB (see Movie S1). The occurrence of EPBs over Brazil for that season was also atypical (Sobral et al., 2002). Therefore, the hypothesis of contributions from recurring penetration of electric fields seems to be reinforced, since both coasts of South America experienced instantaneous occurrences of atypical ESF/EPB events, indicating the action of non-local mechanisms favoring the growth of irregularities over both places.

On the night of August 31–1 September 2021, the irregularity zonal drift over Jicamarca was initially to the east but reversed to west around 23:30 LT (04:37 UT). The images from the all-sky imager in Cachoeira Paulista were cloudy in the early nighttime, but became clear around 04:00 UT. The images reveal an EPB entering the easternmost boundary of the field-of-view of the imager and drifting westward. The time of occurrence is, again, synchronized with that of the westward drifting plume over Jicamarca. Some images from the all-sky imager on that night showing the westward drift of the EPB are presented in Figure 7. The images from São Martinho da Serra (not shown here) are not conclusive, but a visual inspection suggest that no EPBs reached the field-of-view of the instrument on that night. It must be mentioned that these are original images, therefore, some distortion is expected at the edges of the field-of-view of the instrument which might affect proper estimation of the absolute drift velocity. Here, however, the goal is to identify the relative zonal motion (eastward vs. westward). For completeness, sequences of images (movies) are provided as Supporting Information S1 to facilitate the visualization of the dynamics of the EPBs (see Movie S2). Additionally, the reader can access the airglow measurements at https://www2.inpe.br/climaespacial/portal/en/ then select "Products," "All-Sky Imager" where you can choose the station, the date, and verify the original images).

Once again both longitudinal boundaries of the South American continent experienced atypical ESF/EPB simultaneously and with coinciding characteristics. Therefore, a non-local mechanism favoring the ESF/EPB development seems to be the best explanation. Also, since there are distinguishable characteristics between the events on the sequential nights, it is unlikely that a long-term steady contribution such as that from the disturbance dynamo could have caused the events. In addition, it must be mentioned that the prompt penetration electric fields and disturbance dynamo processes are most and least efficient, respectively, during June solstice low solar flux conditions (Fejer et al., 2008; Navarro et al., 2019). Hence, the penetration of electric fields from magnetospheric origin during mild substorms remains as the most likely candidate for the cases evaluated here.

6. On the Possible Mechanisms Leading to the Zonal Drift Reversal

The next question that requires investigation is the cause of the irregularity reversal from east to west on the night of August 31–1 September 2021. According to the discussion in the previous sections, a plausible process that may have led to the occurrence of the irregularities was the penetration of electric fields during mild substorm conditions. If so, the same process operated over both nights, but the resulting temporal behavior of the zonal drifts diverged, that is, reversing from eastward to westward on the second night.

Abdu et al. (1998) used ionosonde data over Fortaleza station to propose a mechanism that, under penetration of zonal electric fields over the equatorial region, could lead to a reversal in the zonal drift. They employed field-aligned integrated quantities (Haerendel et al., 1992) and showed that a combination of Hall conductivity

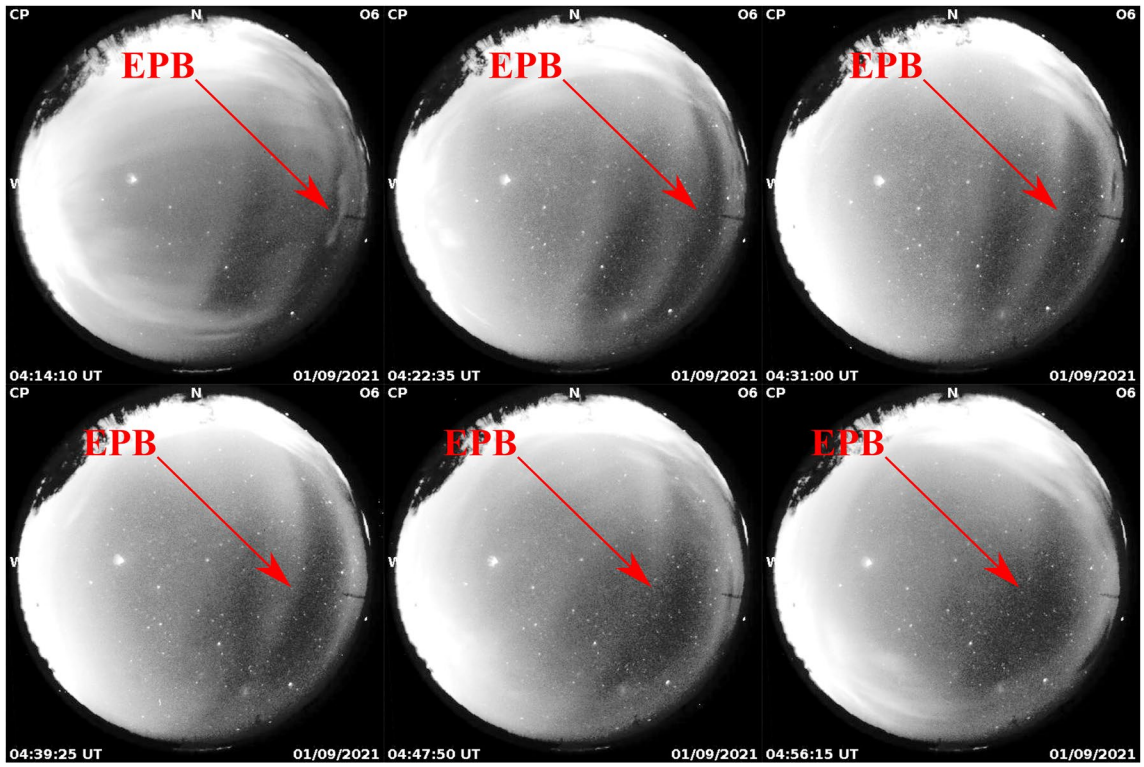

Figure 7. Sequence of images from the all-sky imager deployed at Cachoeira Paulista on August 31– 1 September 2021. The images reveal the westward drift of the Equatorial Plasma Bubble at the same time that the 14-panel Advanced Modular Incoherent Scatter Radar system observed the reversal of the plumes/irregularities over Jicamarca.

and vertical currents originated by diverging horizontal currents could act together (or individually) to originate a reversal in the zonal drift. For the Hall conductivity contribution, the required condition is an enhanced nighttime *E* region conductivity, possibly with gradients (Abdu, 2001), so that the vertical electric field (E_V) can be written in terms of the zonal electric field (E_Z) as:

$$E_V = \left(\frac{\Sigma_H}{\Sigma_P}\right) E_Z, \tag{1}$$

where Σ_H and Σ_P are the field-aligned integrated Hall and Pedersen conductivities. Here, E_Z is assumed as the eastward penetration electric field, and E_V is positive upward.

For the contribution from the vertical current arising due to the divergence in the zonal current, Abdu et al. (1998) proposed that:

$$E_V = -E_Z \int_{90}^{h} \frac{1}{\Sigma_P}\left[\frac{d(\Sigma_P)}{dx}\right] dh, \tag{2}$$

where the integral was assumed to be calculated from 90 km up to an altitude $h > 90$ km, and d/dx corresponds to the derivative in the longitudinal direction.

Abdu et al. (1998) also mentioned that the mechanism proposed could be operative at other longitudes under the conditions described above. In their work they argued that enhanced sporadic *E* (Es) layers could be considered as strong evidence of electron density/E region conductivity enhancements, especially during magnetic disturbances, when particle precipitation over the SAMA region is likely to occur. A sketch of this mechanism is presented in Figure 4 of Abdu et al. (1998). Please notice that Figure 2 demonstrates that the stations used in this work are under the influence of the SAMA, therefore, the mechanism proposed by Abdu et al. (1998) may have been responsible for the irregularity drift reversal.

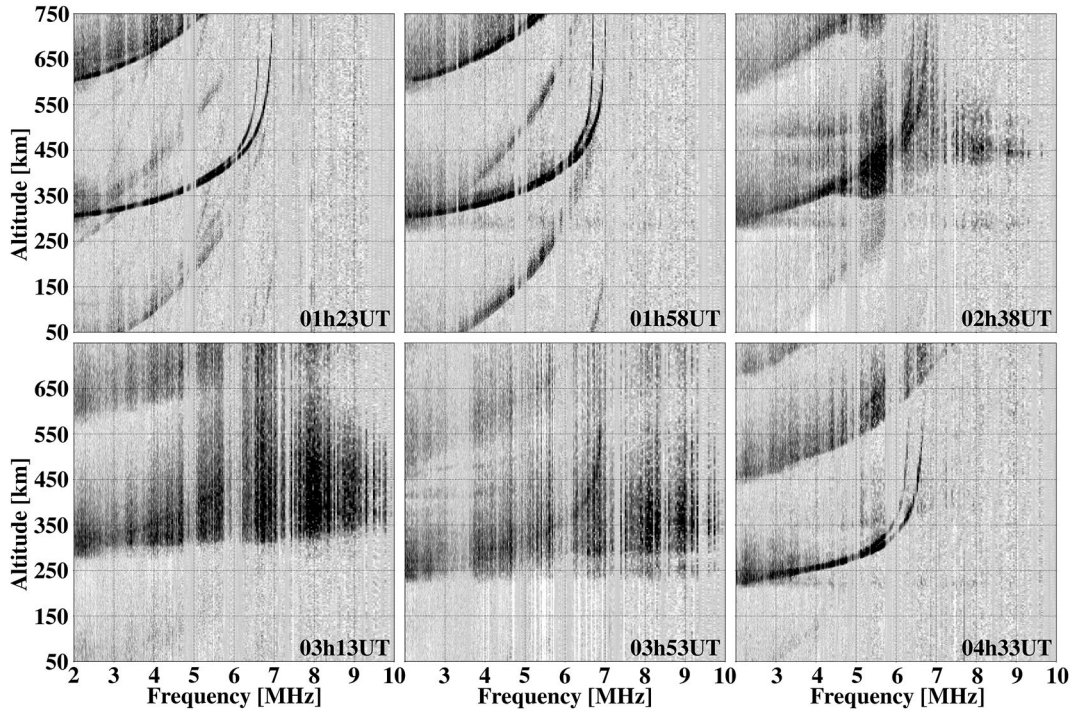

Figure 8. Ionograms over Jicamarca during the time interval in which the plumes were observed by the 14-panel Advanced Modular Incoherent Scatter Radar system on 30–31 August 2021. The plume event that was drifting eastward is manifested in the form of ESF in the ionograms. No noticeable Es layer occurred during this period.

Figure 8 shows six ionograms from the VIPIR ionosonde (Jicamarca) on the night of 30–31 August 2021, between 01:23 UT and 04:33 UT (~20:16 LT–23:26 LT). Please notice that this period covers the hours in which the plume drifting eastward was observed in Figure 3. Hence, the panels in Figure 8 reveal the manifestation of ESF related to the plume captured by the AMISR-14 system and its "disappearance" later at night. During the entire period there are no perceivable occurrences of Es layers in the ionograms. Therefore, it is unlikely that the Hall conductivity required for the mechanism proposed by Abdu et al. (1998) could operate, thus the plume drifted eastward as expected.

Figure 9 shows the VIPIR ionograms over Jicamarca for the night of August 31–1 September 2021, between 02:48 UT and 07:58 UT (~21:41 LT–02:51 LT). Initially, the ionograms did not present Es layers, but around 04:00 UT (~22:53 LT) an Es layer started to develop. This Es layer increased progressively up to about 06:00 UT (~00:53 LT) and faded gradually in later hours.

The first two ionograms correspond to the earliest plume on Figure 5 that was drifting eastward. That plume manifested in the ionograms in the form of ESF. From the third panel on, it is likely that the ESF is related to the second irregularity that was drifting westward in Figure 5. The panels related to the westward irregularity drift (from 04:53 UT on) exhibit noticeable Es layers.

The observations shown in Figures 8 and 9 provide experimental evidence that the mechanism proposed by Abdu et al. (1998) could possibly be the responsible for the reversal, especially the factor related to the Hall conductivity. More specifically, the plume drifted exclusively to the east on the first night, and no Es was noticed at the time when the irregularity occurred. On the second night, the first plume drifted to the east when no Es was present, and the second irregularity observed by the AMISR-14 drifted to the west, simultaneously with the development of Es layers in the ionograms.

As mentioned earlier, the same plume/EPBs drift directions observed over Peru were also detected by the instruments deployed over Brazil, that is, EPBs drifting eastward on August 30–31, 2021 (please see Movie S1 to visualize the dynamics of the EPBs) and westward (at late night) on August 31–September 1, 2021 (Figure 7). Cachoeira Paulista was cloudy on the first night, and the EPB on that night could only be observed by the all-sky in São Martinho da Serra. The closest available Digisonde (Cachoeira Paulista) shows no Es during the interval of the EPB occurrence on August 30–31, 2021 (see Figure S1 in Supporting Information S1). That EPB was drifting

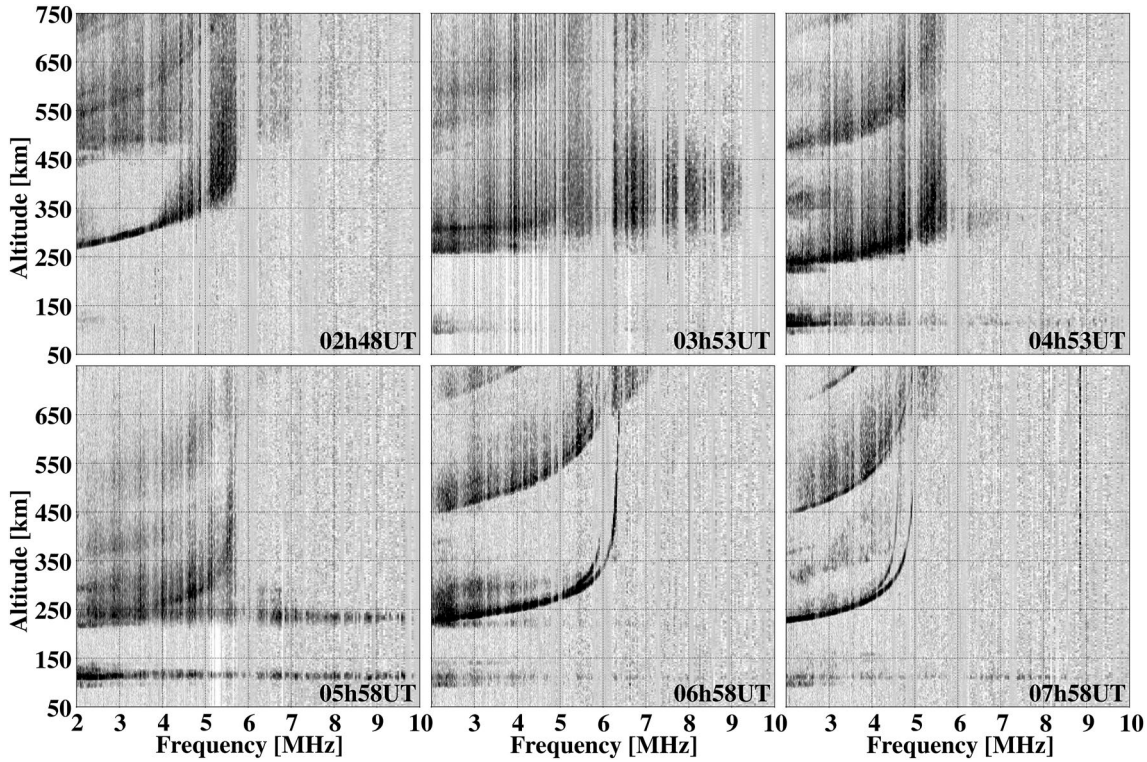

Figure 9. Ionograms over Jicamarca during the time interval in which the plumes were observed by the 14-panel Advanced Modular Incoherent Scatter Radar system on August 31–1 September 2021. The first plume (drifting eastward) is manifested in the form of ESF in the two initial panels. No noticeable Es layer occurred during that period. The second irregularity (drifting westward) is manifested in the form of ESF in the panels corresponding to 04h53 UT and after. An evident Es layer occurred during that period.

eastward and was observed in a region approximately in between Jicamarca and Cachoeira Paulista. Since data over both stations from the VIPIR and Digisonde, respectively, revealed no Es, it is reasonable to assume that no Es occurred at the region where the EPB was observed during that period.

From Figure 7, it is possible to verify that the EPB on the second night entered the easternmost boundary of the field-of-view of the all-sky imager deployed in Cachoeira Paulista at ∼04:00 UT and was drifting westward. The structure was already fully formed, suggesting that it was generated to the east of that geomagnetic meridian, therefore, data from the Digisondes deployed at Fortaleza and São Luís were also employed to evaluate the ionospheric conditions in geomagnetic meridians slightly to the east of Cachoeira Paulista. Figure 10 shows some ionograms from Fortaleza (upper panels) and São Luís (middle panels) around the period when the EPB was observed by the all-sky in Cachoeira Paulista on August 31–1 September 2021. Both stations experienced strong Es occurrence during that period.

According to the images in Figure 7, the EPB was expected to reach Cachoeira Paulista (i.e., the center of the image) after 05:00 UT, for that reason the lower panels in Figure 10 also display some ionograms over Cachoeira Paulista between 05:30 UT and 07:00 UT. During that period, noticeable Es layers were also occurring over Cachoeira Paulista. The hours covered by the panels of Figure 10 are approximately the same in which the irregularity drifting westward was observed by the AMISR-14 radar beams over Jicamarca.

There are three main aspects in the results discussed above that support the hypothesis that the mechanism proposed by Abdu et al. (1998) led to the reversal in the irregularity/EPB zonal drift: (a) during the night with plumes/EPB drifting eastward over Peru and Brazil (e.g., Figure 3 and Movie S1), observations from instruments in both regions did not show evidence of Es layers; (b) on the second night, the first plume over Jicamarca was drifting eastward and no Es was observed, but the subsequent irregularity structure started to drift westward immediately after the appearance of Es layers over Peru; and (c) over Brazil, the EPB observed was drifting westward exactly at the same time when Jicamarca observed the reversal in the zonal drift. The Digisondes over the Brazilian region also revealed the development of Es layers at that time.

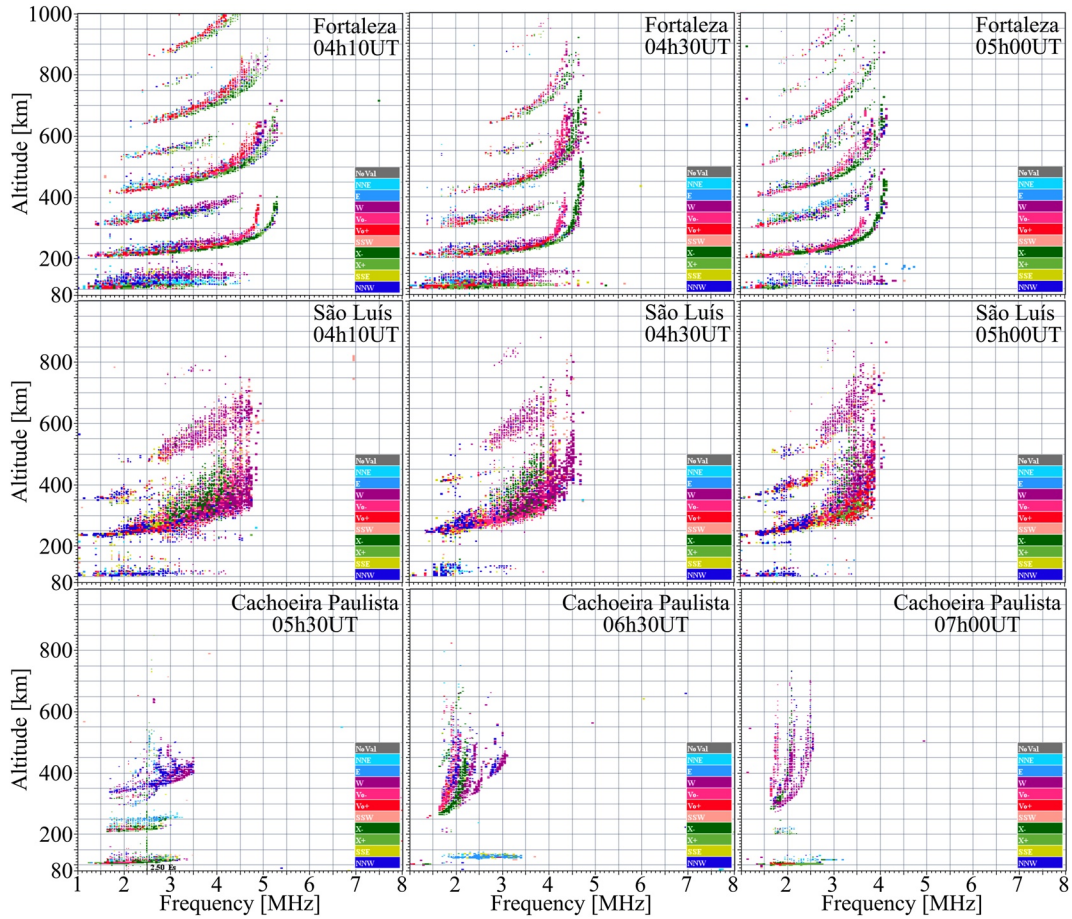

Figure 10. Ionograms from Fortaleza (upper panels), São Luís (middle panels), and Cachoeira Paulista (lower panels). Over Fortaleza and São Luís noticeable Es layers were observed during the Equatorial Plasma Bubble (EPB) westward drift around their respective geomagnetic meridians. Later hours are exhibited in panels for Cachoeira Paulista because the EPB only reached that region after 05:00 UT according to Figure 7. The Es occurrence is also evident over Cachoeira Paulista at that period. The time interval covered in this figure coincides with that of the irregularity drifting westward observed over Jicamarca.

Abdu et al. (1998) used ionosonde data from Fortaleza, close to the eastern boundary of the SAMA, when evaluating the mechanism proposed in their work. Due to this, a decrease in electron density was expected as locations further east were considered. Consequently, the right-hand side of Equation 2 would be positive, therefore, a positive E_Z would imply an upward E_V. For Jicamarca the situation is the opposite, therefore, if the increase in the electron densities was caused by particle precipitation around the SAMA region as suggested by Abdu et al. (1998), it is likely that an upsurge in the Hall conductivity contribution (Equation 1) is the main mechanism causing the reversal. Otherwise, the contributions from the Hall conductivity and the vertical current (Equation 2) would have opposite directions over Jicamarca, decreasing the efficiency of the mechanism.

The comparison of results over Peruvian and Brazilian regions is suitable to evaluate the mechanism proposed by Abdu et al. (1998) because the observations cover, approximately, the westernmost and the easternmost boundaries of the South Atlantic Magnetic Anomaly. Consequently, although the vertical current is theoretically expected to contribute to the mechanism evaluated, the results for the two nights presented in this work suggest that its contribution was secondary, and the Hall conductivity term dominates.

7. Conclusion

The AMISR-14 radar observed the development of plumes over Jicamarca on two consecutive nights during the solar minimum (85.7 sfu $\leq F10.7 \leq$ 92.4 sfu), June solstice period (August 30–31, 2021, and August 31–1

September 2021), under geomagnetic conditions that are often classified as "quiet." Consequently, these plume/EPB occurrences are atypical, given the unfavorable seasonal conditions for that station. More interestingly, the AMISR-14 system capability of observing from distinct pointing directions allowed the identification of a reversal in the irregularity zonal drift on the second night. These observations motivated a multi-instrumental and multi-location investigation to understand the processes favoring the development of plumes/EPBs under adverse seasonal conditions and the mechanisms that may have led to the reversal of the irregularity zonal drift on the second night. Data from instruments deployed over the Peruvian and Brazilian regions were used to evaluate the generation and the zonal drift of the plumes/EPBs on both nights over both locations.

The main results of this investigation can be summarized as follows:

1) The AMISR-14 data can be used to produce 2D representations of the plumes around Jicamarca, providing information well-suited for studies of their generation, dynamics, and decay.
2) Under southward B_Z conditions, the augmentation in the eastward E_y seems to be promptly connected to the equatorial region, contributing to the changes in the vertical component of the plasma drift, as revealed by the resemblances between the profiles of these quantities on both nights.
3) Even during nights under very mild geomagnetic perturbations, the recurring occurrence of substorms and penetration of electric fields in the equatorial ionosphere seems to be a process that can drive substantial changes in the electrodynamics over that region. These changes can, possibly, favor the development of ESF.
4) The analysis of data from several instruments located at opposite coasts of the South American continent revealed that it is likely that the processes favoring the occurrence of plumes/EPBs and the reversal of the zonal drift on the second night were non-local, reinforcing the hypothesis of a contribution from the penetration electric fields.
5) This work confirms that the mechanism proposed by Abdu et al. (1998) is well-suited to explain the reversal in the irregularity zonal drift simultaneously over distinct longitudes. The description given by their work and the results presented here for both nights and over both locations match noticeably well, especially with regards to the contribution of the Hall conductivity term (Equation 1).
6) The analysis of data from opposite "boundaries" of the SAMA suggests that, for the events evaluated in this work, the contribution from the vertical current term to the reversal in the zonal drift was negligible, despite expectations from theory.

Data Availability Statement

IGRF13 can be accessed at https://www.ngdc.noaa.gov/IAGA/vmod/igrf.html. The solar flux, Dst and Kp indices can be accessed at https://omniweb.gsfc.nasa.gov. The AE index can be accessed at https://wdc.kugi.kyoto-u.ac.jp/ae_realtime/index.html. The substorm timing list can be accessed at https://supermag.jhuapl.edu/substorms/. The all-sky imager and Digisonde data can be accessed at https://www2.inpe.br/climaespacial/portal/en/. The VIPIR data can be accessed at http://lisn.igp.gob.pe/. The AMISR-14 data used is available at (Sousasantos et al., 2023).

Acknowledgments
Research at UT Dallas was supported by NSF awards AGS-1916055 and AGS-2122639. B. G. Fejer acknowledges NASA H-LWS program through Grant 80NSSC17K071. C. E. Valladares was supported by Grant AGS-1933056 and NASA Grants 80NSSC20K0195 and 80NSSC20K177. Authors would like to thank the International Association of Geomagnetism and Aeronomy (IAGA) and all the scientific and technical staff responsible for the distribution of the International Geomagnetic Reference Field (IGRF). The authors acknowledge the NASA Space Physics Data Facility staff. The OMNI data were obtained from the GSFC/SPDF OMNIWeb interface at https://omniweb.gsfc.nasa.gov. We are also grateful to the EMBRACE (Estudo e Monitoramento Brasileiro do Clima Espacial) from the National Institute for Space Research (INPE), to the Low-Latitude Ionospheric Sensor Network (LISN), and to the Global Ionospheric Radio Observatory (GIRO) from the University of Massachusetts Lowell Center for Atmospheric Research (UMLCAR). The Low Latitude Ionospheric Sensor Network (LISN) is funded by NSF Grant AGS-1933056 and is a project led by UT Dallas in collaboration with the Instituto Geofísico del Perú and other institutions that provide information in benefit of the space weather scientific community. The Jicamarca Radio Observatory is a facility of the Instituto Geofísico del Perú operated with support from the NSF AGS-2213849 through Cornell University. We acknowledge the substorm timing list (available at https://supermag.jhuapl.edu/substorms/) identified by the Newell and Gjerloev (Newell & Gjerloev, 2011) and Ohtani and Gjerloev (2020) techniques and the SuperMAG collaboration (Gjerloev, 2012).

References

Abdu, M. A. (2001). Outstanding problems in the equatorial ionosphere–thermosphere electrodynamics relevant to spread F. *Journal of Atmospheric and Solar-Terrestrial Physics*, *63*(9), 869–884. https://doi.org/10.1016/S1364-6826(00)00201-7

Abdu, M. A., Batista, I. S., Reinisch, B. W., de Souza, J. R., Sobral, J. H. A., Pedersen, T. R., et al. (2009). Conjugate point equatorial experiment (COPEX) campaign in Brazil: Electrodynamics highlights on spread F development conditions and day-to-day variability. *Journal of Geophysical Research*, *114*(A4), 1–21. https://doi.org/10.1029/2008JA013749

Abdu, M. A., Batista, I. S., Takahashi, H., MacDougall, J., Sobral, J. H. A., Medeiros, A. F., & Trivedi, N. B. (2003). Magnetospheric disturbance induced equatorial plasma bubble development and dynamics: A case study in Brazilian sector. *Journal of Geophysical Research*, *108*(A12), 1–13. https://doi.org/10.1029/2002JA009721

Abdu, M. A., de Medeiros, R. T., Bittencourt, J. A., & Batista, I. S. (1983). Vertical ionization drift velocities and range type spread F in the evening equatorial ionosphere. *Journal of Geophysical Research*, *88*(A1), 399–402. https://doi.org/10.1029/JA088iA01p00399

Abdu, M. A., Jayachandran, T., MacDougall, J., Cecile, J. F., & Sobral, J. H. A. (1998). Equatorial F region zonal plasma irregularity drifts under magnetospheric disturbances. *Geophysical Research Letters*, *25*(22), 4137–4140. https://doi.org/10.1029/1998GL900117

Ajith, K. K., Tulasi Ram, S., Yamamoto, M., Otsuka, Y., & Niranjan, K. (2016). On the fresh development of equatorial plasma bubbles around the midnight hours of June solstice. *Journal of Geophysical Research: Space Physics*, *121*(9), 9051–9062. https://doi.org/10.1002/2016JA023024

Ajith, K. K., Tulasi Ram, S., Yamamoto, M., Yokoyama, T., Sai Gowtam, V., Otsuka, Y., et al. (2015). Explicit characteristics of evolutionary-type plasma bubbles observed from Equatorial Atmosphere Radar during the low to moderate solar activity years 2010–2012. *Journal of Geophysical Research: Space Physics*, *120*(2), 1371–1382. https://doi.org/10.1002/2014JA020878

Alken, P., Thébault, E., Beggan, C. D., Amit, H., Aubert, J., Baerenzung, J., et al. (2021). International geomagnetic reference field: The thirteenth generation. *Earth Planets and Space*, *73*(49), 1–25. https://doi.org/10.1186/s40623-020-01288-x

Blanc, M., & Richmond, A. D. (1980). The ionospheric disturbance dynamo. *Journal of Geophysical Research*, *85*(A4), 1669–1686. https://doi.org/10.1029/JA085iA04p01669

Chandra, H., & Rastogi, R. G. (1972). Spread-F at magnetic equatorial station Thumba. *Annales Geophysicae*, *28*, 37–44.

Chapagain, N. P., Fejer, B. G., & Chau, J. L. (2009). Climatology of postsunset equatorial spread F over Jicamarca. *Journal of Geophysical Research*, *114*(A7), 1–7. https://doi.org/10.1029/2008JA013911

Fejer, B. G., Blanc, M., & Richmond, A. D. (2017). Post-storm middle and low-latitude ionospheric electric field effects. *Space Science Reviews*, *206*(1–4), 407–429. https://doi.org/10.1007/s11214-016-0320-x

Fejer, B. G., Jensen, J. W., & Su, S.-Y. (2008). Seasonal and longitudinal dependence of equatorial disturbance vertical plasma drifts. *Geophysical Research Letters*, *35*(20), 1–4. https://doi.org/10.1029/2008GL035584

Fejer, B. G., Kudeki, E., & Farley, D. T. (1985). Equatorial F region zonal plasma drifts. *Journal of Geophysical Research*, *90*(A12), 12249–12255. https://doi.org/10.1029/JA090iA12p12249

Fejer, B. G., & Navarro, L. A. (2022). First observations of equatorial ionospheric electric fields driven by storm-time rapidly recurrent magnetospheric substorms. *Journal of Geophysical Research: Space Physics*, *127*(12), 1–8. https://doi.org/10.1029/2022JA030940

Fejer, B. G., Navarro, L. A., Sazykin, S., Newheart, A., Milla, M. A., & Condor, P. (2021). Prompt penetration and substorm effects over Jicamarca during the September 2017 geomagnetic storm. *Journal of Geophysical Research: Space Physics*, *126*(8), 1–11. https://doi.org/10.1029/2021JA029651

Fejer, B. G., & Scherliess, L. (1998). Mid- and low-latitude prompt penetration ionospheric zonal plasma drifts. *Geophysical Research Letters*, *25*(16), 3071–3074. https://doi.org/10.1029/98GL02325

Fejer, B. G., Tracy, B. D., & Pffaf, R. F. (2013). Equatorial zonal plasma drifts measured by the C/NOFS satellite during the 2008-2011 solar minimum. *Journal of Geophysical Research: Space Physics*, *118*(6), 3891–3897. https://doi.org/10.1002/jgra.50382

Gjerloev, J. W. (2012). The SuperMAG data processing technique. *Journal of Geophysical Research*, *117*(A9), 1–19. https://doi.org/10.1029/2012JA017683

Haerendel, G., Eccles, J. V., & Çakir, S. (1992). Theory for modeling the equatorial evening ionosphere and the origin of the shear in the horizontal plasma flow. *Journal of Geophysical Research*, *97*(A2), 1209–1223. https://doi.org/10.1029/91JA02226

Huang, C. S. (2018). Effects of the postsunset vertical plasma drift on the generation of equatorial spread F. *Progress in Earth and Planetary Science*, *5*(3), 1–15. https://doi.org/10.1186/s40645-017-0155-4

Jayachandran, B., Balan, N., Rao, B., Sastri, J. H., & Bailey, G. J. (1993). HF doppler and ionosonde observations on the onset conditions of equatorial spread F. *Journal of Geophysical Research*, *98*(A8), 13741–13750. https://doi.org/10.1029/93JA00302

Kelley, M. C. (1989). *The Earth's ionosphere: Plasma physics and electrodynamics* (Vol. 43). Academic Press.

King, J. H., & Papitashvili, N. E. (2005). Solar wind spatial scales in and comparisons of hourly Wind and ACE lasma and magnetic field data. *Journal of Geophysical Research*, *110*(A2), 1–8. https://doi.org/10.1029/2004JA010649

Li, G., Ning, B., Abdu, M. A., Yue, X., Liu, L., Wan, W., & Hu, L. (2011). On the occurrence of postmidnight equatorial F region irregularities during the June solstice. *Journal of Geophysical Research*, *116*(A4), 1–19. https://doi.org/10.1029/2010JA016056

Loewe, C. A., & Prölss, G. W. (1997). Classification and mean behavior of magnetic storms. *Journal of Geophysical Research*, *102*(A7), 14209–14213. https://doi.org/10.1029/96JA04020

Navarro, L. A., & Fejer, B. G. (2019). Storm-time thermospheric winds over Peru. *Journal of Geophysical Research: Space Physics*, *124*(12), 10415–10427. https://doi.org/10.1029/2019JA027256

Navarro, L. A., & Fejer, B. G. (2020). Storm-time coupling of equatorial nighttime F region neutral winds and plasma drifts. *Journal of Geophysical Research: Space Physics*, *125*(9), 1–10. https://doi.org/10.1029/2020JA028253

Navarro, L. A., Fejer, B. G., & Scherliess, L. (2019). Equatorial disturbance dynamo vertical plasma drifts over Jicamarca: Bimonthly and solar cycle dependence. *Journal of Geophysical Research: Space Physics*, *124*(6), 4833–4841. https://doi.org/10.1029/2019JA026729

Newell, T., & Gjerloev, J. W. (2011). Substorm and magnetosphere characteristic scales inferred from the SuperMAG auroral electrojet indices. *Journal of Geophysical Research*, *116*(A12), 1–15. https://doi.org/10.1029/2011JA016936

Ohtani, S., & Gjerloev, J. W. (2020). Is the substorm current wedge an ensemble of wedgelets? Revisit to midlatitude positive bays. *Journal of Geophysical Research: Space Physics*, *125*(9), 1–16. https://doi.org/10.1029/2020JA027902

Ossakow, S. L., Zalesak, S. T., McDonald, B. E., & Chaturvedi, P. K. (1979). Nonlinear equatorial spread F: Dependence on altitude of the F peak and bottomside background electron density gradient scale length. *Journal of Geophysical Research*, *84*(A1), 17–29. https://doi.org/10.1029/JA084iA01p00017

Patra, A. K., Phanikumar, D. V., & Pant, T. K. (2009). Gadanki radar observations of F region field-aligned irregularities during June solstice of solar minimum: First results and preliminary analysis. *Journal of Geophysical Research*, *114*(A12), 1–10. https://doi.org/10.1029/2009JA014437

Paulino, I., Medeiros, A. F., Buriti, R. A., Sobral, J. H. A., Takahashi, H., & Gobbi, D. (2010). Optical observations of plasma bubble westward drifts over Brazilian tropical region. *Journal of Atmospheric and Solar-Terrestrial Physics*, *72*(5–6), 521–527. https://doi.org/10.1016/j.jastp.2010.01.015

Rodrigues, F. S., Hickey, D. A., Zhan, W., Martinis, C. R., Fejer, B. G., Milla, M., & Arratia, J. F. (2018). Multi-instrumented observations of the equatorial F-region during June solstice: Large-scale wave structures and spread-F. *Progress in Earth and Planetary Science*, *5*(14), 1–16. https://doi.org/10.1186/s40645-018-0170-0

Rodrigues, F. S., Nicolls, M. J., Milla, M. A., Smith, J. M., Varney, R. H., Strømme, A., et al. (2015). AMISR-14: Observations of equatorial spread F. *Geophysical Research Letters*, *42*(13), 5100–5108. https://doi.org/10.1002/2015GL064574

Sastri, J. H. (1999). Post-midnight onset of spread-F at Kodaikanal during the June solstice of solar minimum. *Annales Geophysicae*, *17*(8), 1111–1115. https://doi.org/10.1007/s00585-999-1111-4

Scherliess, L., & Fejer, B. G. (1999). Radar and satellite global equatorial F region vertical drift model. *Journal of Geophysical Research*, *104*(A4), 6829–6842. https://doi.org/10.1029/1999JA900025

Senior, C., & Blanc, M. (1984). On the control of magnetospheric convection by the spatial distribution of ionospheric conductivities. *Journal of Geophysical Research*, *89*(A1), 261–284. https://doi.org/10.1029/JA089iA01p00261

Shidler, S. A., Rodrigues, F. S., Fejer, B. G., & Milla, M. A. (2019). Radar studies of height-dependent equatorial F region vertical and zonal plasma drifts. *Journal of Geophysical Research: Space Physics*, *124*(3), 2058–2071. https://doi.org/10.1029/2019JA026476

Smith, J. M., Rodrigues, F. S., Fejer, B. G., & Milla, M. A. (2016). Coherent and incoherent scatter radar study of the climatology and day-to-day variability of mean F region vertical drifts and equatorial spread F. *Journal of Geophysical Research: Space Physics*, *121*(2), 1466–1482. https://doi.org/10.1002/2015JA021934

Sobral, J. H. A., Abdu, M. A., Takahashi, H., Taylor, M. J., de Paula, E. R., Zamlutti, C. J., et al. (2002). Ionospheric plasma bubble climatology over Brazil based on 22 years (1977-1998) of 630 nm airglow observations. *Journal of Atmospheric and Solar-Terrestrial Physics*, *64*(12–14), 1517–1524. https://doi.org/10.1016/S1364-6826(02)00089-5

Sobral, J. H. A., Castilho, M., Abdu, M. A., Takahashi, H., Paulino, I., Gasparelo, U. A. C., et al. (2011). Midnight reversal of ionospheric plasma bubble eastward velocity to westward velocity during geomagnetically quiettime: Climatology and its model validation. *Journal of Atmospheric and Solar-Terrestrial Physics*, *73*(11–12), 1520–1528. https://doi.org/10.1016/j.jastp.2010.11.031

Sousasantos, J., Rodrigues, F. S., Fejer, B. G., Abdu, M. A., Massoud, A. A., & Valladares, C. E. (2023). On the role of mild substorms and enhanced Hall conductivity in the plasma irregularities onset and zonal drift reversals: Experimental evidence at distinct longitudes over South America [Dataset]. Zenodo. https://doi.org/10.5281/zenodo.10023316

Spiro, R. W., Wolf, R. A., & Fejer, B. G. (1988). Penetrating of high-latitude-electric-field effects to low latitudes during SUNDIAL 1984. *Annales Geophysicae*, *6*, 39–49.

Subbarao, K. S. V., & Krishnamurthy, B. V. (1994). Seasonal variations of equatorial spread-F. *Annales Geophysicae*, *12*(1), 33–39. https://doi.org/10.1007/s005850050033

Sultan, J. (1996). Linear theory and modeling of the Rayleigh-Taylor instability leading to the occurrence of equatorial spread F. *Journal of Geophysical Research*, *101*(A12), 26875–26891. https://doi.org/10.1029/96JA00682

Valladares, C. E., Sheehan, R., Basu, S., Kuenzler, H., & Espinoza, J. (1996). The multi-instrumented studies of equatorial thermosphere aeronomy scintillation system: Climatology of zonal drifts. *Journal of Geophysical Research*, *101*(A12), 26839–26850. https://doi.org/10.1029/96JA00183

Vargas, F., Brum, C. G. M., Terra, P., & Gobbi, D. (2020). Mean zonal drift velocities of plasma bubbles estimated from keograms of nightglow all-sky images from the Brazilian sector. *Atmosphere*, *11*(1), 1–9. https://doi.org/10.3390/atmos11010069

Yizengaw, E., Retterer, J., Pacheco, E. E., Roddy, P., Groves, K., Caton, R., & Baki, P. (2013). Postmidnight bubbles and scintillations in the quiet-time June solstice. *Geophysical Research Letters*, *40*(21), 5592–5597. https://doi.org/10.1002/2013GL058307

Zhan, W., & Rodrigues, F. S. (2018). Solstice equatorial spread F in the American sector: A numerical assessment of linear stability aided by Incoherent Scatter Radar measurements. *Journal of Geophysical Research: Space Physics*, *123*(1), 755–767. https://doi.org/10.1002/2017JA024969